small methods
www.small-methods.com

Spectroscopic and Biophysical Methods to Determine Differential Salt-Uptake by Primitive Membraneless Polyester Microdroplets

Chen Chen, Ruiqin Yi, Motoko Igisu, Chie Sakaguchi, Rehana Afrin, Christian Potiszil, Tak Kunihiro, Katsura Kobayashi, Eizo Nakamura, Yuichiro Ueno, André Antunes, Anna Wang, Kuhan Chandru, Jihua Hao, and Tony Z. Jia**

α-Hydroxy acids are prebiotic monomers that undergo dehydration synthesis to form polyester gels, which assemble into membraneless microdroplets upon aqueous rehydration. These microdroplets are proposed as protocells that can segregate and compartmentalize primitive molecules/reactions. Different primitive aqueous environments with a variety of salts could have hosted chemistries that formed polyester microdroplets. These salts could be essential cofactors of compartmentalized prebiotic reactions or even directly affect protocell structure. However, fully understanding polyester–salt interactions remains elusive, partially due to technical challenges of quantitative measurements in condensed phases. Here, spectroscopic and biophysical methods are applied to analyze salt uptake by polyester microdroplets. Inductively coupled plasma mass spectrometry is applied to measure the cation concentration within polyester microdroplets after addition of chloride salts. Combined with methods to determine the effects of salt uptake on droplet turbidity, size, surface potential and internal water distribution, it was observed that polyester microdroplets can selectively partition salt cations, leading to differential microdroplet coalescence due to ionic screening effects reducing electrostatic repulsion forces between microdroplets. Through applying existing techniques to novel analyses related to primitive compartment chemistry and biophysics, this study suggests that even minor differences in analyte uptake can lead to significant protocellular structural change.

1. Introduction

On prebiotic Earth, the heterogeneous milieu contained a high diversity of organic chemicals (and related reactions), including both biotic and abiotic compounds.[1,2] In particular, abiotic molecules, i.e., those not commonly used by extant biology, may have played an important role in prebiotic chemistries and could have assisted evolving primitive chemical systems.[2,3] α-Hydroxy acids (αHAs), monomers with structures similar to α-amino acids, are one type of abundant abiotic monomer likely present on early Earth;[2,4] αHAs could have arisen from plausible prebiotic mechanisms such as terrestrial spark discharge,[5] hydrothermal environment reactions,[6] delivery via extraterrestrial carbonaceous meteorites[7] or ultraviolet photochemistry.[8]

Solutions containing αHAs can undergo dehydration to yield gel-like polyesters in conditions that mimic aqueous environments on early Earth.[9,10] After rehydration in aqueous medium, polyesters can assemble into membraneless droplets via liquid–liquid phase

C. Chen, R. Yi, R. Afrin, Y. Ueno, T. Z. Jia
Earth-Life Science Institute
Tokyo Institute of Technology
Meguro-ku, Tokyo 152-8550, Japan
E-mail: chenchen@elsi.jp; tzjia@elsi.jp

M. Igisu, Y. Ueno
Institute for Extra-cutting-edge Science and Technology Avant-garde Research (X-star)
Japan Agency for Marine-Earth Science and Technology (JAMSTEC)
Yokosuka, Kanagawa 237-0061, Japan

C. Sakaguchi, C. Potiszil, T. Kunihiro, K. Kobayashi, E. Nakamura
The Pheasant Memorial Laboratory for Geochemistry and Cosmochemistry
Institute for Planetary Materials
Okayama University
Misasa, Tottori 682-0193, Japan

Y. Ueno
Department of Earth and Planetary Sciences
Tokyo Institute of Technology
Meguro-ku, Tokyo 152-8551, Japan

The ORCID identification number(s) for the author(s) of this article can be found under https://doi.org/10.1002/smtd.202300119

DOI: 10.1002/smtd.202300119

separation (LLPS), a physicochemical phase transition phenomenon in which a homogeneous liquid spontaneously demixes into two or more coexisting liquids.[11] Membraneless droplets, such as polyester microdroplets,[12,13] biomolecular coacervates[14–16] or aqueous two-phase systems (ATPS),[17] were first proposed as model protocells by Oparin and Haldane in the 1920s[12,13,18–20] and in particular, membraneless protocells are hypothesized to have preceded membrane-bound protocells.[21]

Membraneless protocells themselves exhibit a variety of dynamic behaviors that may indicate or be associated with life, such as material exchange,[22] mobility,[23] coalescence and surface wetting,[24] analyte concentration[25] and enhancement of compartmentalized analyte catalytic activity.[26] In fact, modern cells also contain many membraneless organelles generated by LLPS that have essential structural, catalytic and regulatory roles, while aberrant intracellular phase separation can even cause neurodegenerative diseases.[27–29] Thus, the importance of membraneless compartments in modern biology, coupled with the potential importance of membraneless protocells, suggests that LLPS may structurally or functionally connect the origin of life to modern biology.

Modern life is water-dependent, and given the existence of different aqueous environments on Earth, it has also been hypothesized that life originated and evolved in ancient aqueous environments.[30] Thus, the structure of membraneless protocells would then depend sensitively on environmental factors that affected primitive aqueous chemistries, such as temperature and pressure,[31,32] salts[33] and pH,[34] etc. In particular, dissolved salts are present in seawater, including those composed of cations such as sodium (Na^+), potassium (K^+), magnesium (Mg^{2+}), and calcium (Ca^{2+}) and anions such as chloride (Cl^-),[35] and would have also been present in the ancient ocean,[36] although at different concentrations than the modern day. The same ions also have multiple roles in modern life, including as electrical communication regulators (Na^+, K^+ and Ca^{2+}),[37] protein cofactors (Mg^{2+})[38] or cellular stimulus-response controllers (Cl^-).[39]

Salts not only affect extant biology, but also affect membraneless protocell properties. For example, the structure of biphasic ssDNA–peptide–quaternized dextran coacervate droplets can be tuned by NaCl, resulting in subcompartment fusion;[40] modulation of NaCl concentration drives the emergence of liquid crystal phase transitions in dsDNA–peptide coacervates;[41] and membraneless protein droplets that generally phase separate only at low KCl concentrations can also re-enter a phase separated state at high KCl concentrations.[33] Previously, it was observed that NaCl could induce polyester microdroplet coalescence, although the mechanism is not yet known.[12] In general, how salt ions influence polyester microdroplet phase behavior or salt–polyester interactions in a prebiotic context and whether polyester microdroplets can selectively partition different salts have not been well studied. Thus, we sought to characterize the ability for polyester microdroplets to uptake salt ions, as well as the effects of salt uptake on physical microdroplet properties such as coalescence and surface charge. Further elucidation of the physical properties of membraneless protocell models may help to answer the many unanswered questions related to the use of membraneless phase-separated droplets as model protocell systems, such as the emergence of "life-like" functions including partitioning, stability or evolution.[42]

To mimic the messy prebiotic chemical milieu, we first subject a series of αHAs to dehydration synthesis to form polyesters, which were then subsequently screened for microdroplet assembly.[43] Based on their significant propensity to form droplets after synthesis, DL-3-phenyllactic acid (PA) was chosen as the model αHA of choice for this study.[12] However, given that salt–polyester interactions (which could govern salt uptake) may be significantly affected by electrostatic interactions, incorporation of basic or acidic αHA residues into a polyester chain could result in differential interactions with salts, as compared to a fully neutral polyester such as poly(PA). Previously, primitive polyesters containing basic (S)-(-)-4-amino-2-hydroxybutyric acid (4a2h) and acidic DL-malic acid (Malic) has been demonstrated.[13,44] Thus, our αHA library consisted of PA, 4a2h and Malic, and we produced polyester microdroplets composed of both homopolyesters (poly(PA)) and potentially charged heteropolyesters (poly(Malic-PA) and poly(4a2h-PA)) for downstream analysis.

Inductively coupled plasma mass spectrometry (ICP-MS) can detect ions or metals (e.g., in extraterrestrial asteroid samples) and can simultaneously measure multiple elements with high sensitivity.[45] We thus applied a novel ICP-MS-based analytical approach to determine the cation distribution within polyester microdroplets following incubation with four different chloride salts (NaCl, KCl, $MgCl_2$ and $CaCl_2$; all present in early oceans). We also conducted in parallel a series of biophysical measurements on the turbidity, size, water distribution and surface

A. Antunes
State Key Laboratory of Lunar and Planetary Sciences
Macau University of Science and Technology (MUST)
Taipa, Macau, SAR, China
A. Antunes, J. Hao, T. Z. Jia
Blue Marble Space Institute of Science
Seattle, WA 98104, USA
A. Wang
School of Chemistry
UNSW Sydney
Sydney, NSW 2052, Australia
A. Wang
Australian Centre for Astrobiology
UNSW Sydney
Sydney, NSW 2052, Australia
A. Wang
RNA Institute
UNSW Sydney
Sydney, NSW 2052, Australia
A. Wang
ARC Centre of Excellence for Synthetic Biology
UNSW Sydney
Sydney, NSW 2052, Australia
K. Chandru
Space Science Center (ANGKASA)
Institute of Climate Change
National University of Malaysia
Selangor 43650, Malaysia
J. Hao
Deep Space Exploration Laboratory/CAS Laboratory of Crust-Mantle Materials and Environments
University of Science and Technology of China
Hefei 230026, China

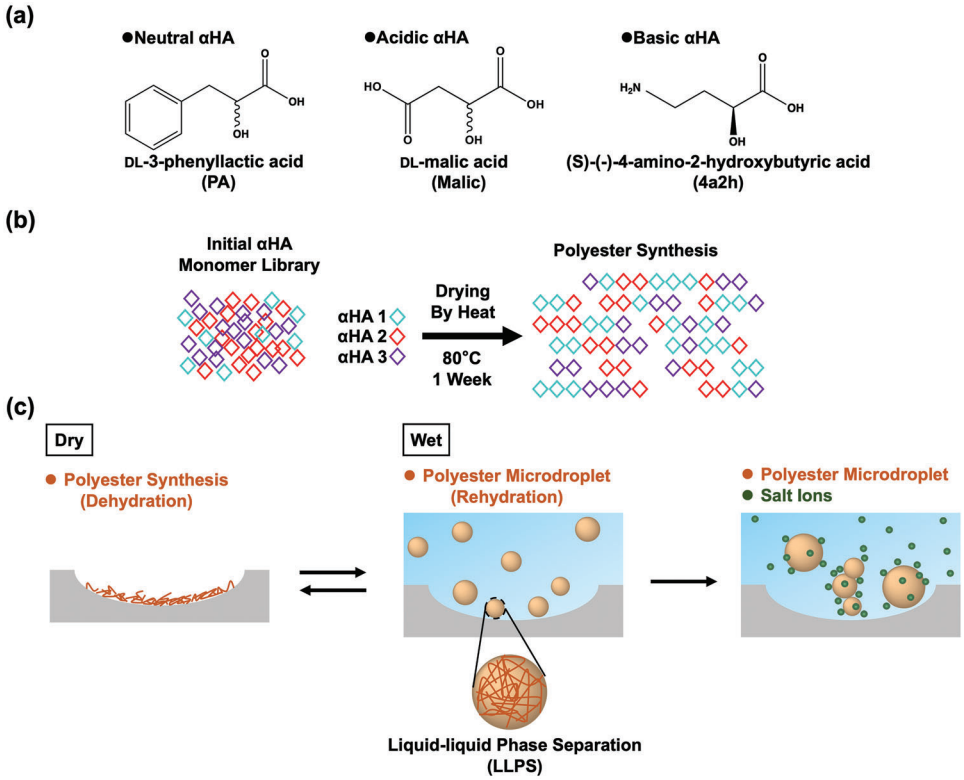

Figure 1. a) Chemical structure of the three αHAs studied. b) Polyester synthesis from dehydration of αHA monomers. c) Polyester microdroplet formation after rehydration and their coexistence with and/or uptake of salt ions.

potential of the droplets to correlate the physical effects resulting from salt uptake within the polyester microdroplets (**Figure 1**). We observed that polyester microdroplets can selectively partition salt cations, leading to differential microdroplet coalescence due to ionic screening effects reducing electrostatic repulsion forces between microdroplets. To our knowledge, this is the first application of ICP-MS to understanding the biophysics of a nonassociative membraneless protocell system (i.e., polyester microdroplets) in the origins of life field. These findings suggest that even minor differences in analyte uptake by primitive compartments could result in significant protocellular structural changes, leading to potential chemical evolution of protocell systems in prebiotic aqueous environments.

2. Results and Discussion

2.1. Polyester Dehydration Synthesis and Microdroplet Assembly via Rehydration

Previous studies have shown that synthesized polyesters composed of poly(PA) and 1:1 4a2h/PA can undergo droplet assembly. Dehydration synthesis of pure 4a2h resulted in polymerization, but not microdroplet formation,[13] while increasing amounts 4a2h incorporated into PA-containing polyesters resulted in increased solubility and a lower tendency of droplet assembly.[13] However, polyester droplets composed of Malic/PA have not yet been demonstrated. We thus subjected pure PA and Malic solutions, as well as 1:1 Malic/PA and 1:1 4a2h/PA solutions, to dehydration synthesis to generate homo- and heteropolyester products. The resulting polyester products reached lengths of up to 20 residues depending on the droplet composition as analyzed by matrix-assisted laser desorption ionization time-of-flight mass spectrometry (MALDI-TOF-MS). The homopolyesters poly(PA) and poly(Malic) were detected from pure PA or Malic monomer reactions (**Figure 2**a; Figure S1 and Tables S1 and S2, Supporting Information). The heteropolyesters poly(Malic-PA) and poly(4a2h-PA) were also detected as products of the respective reactions starting from mixed monomer solutions (Figure 2b,c; Tables S3 and S4, Supporting Information), suggesting co-incorporation of all monomers present in the initial reaction mixtures.

We then characterized the phase separation properties of the synthesized polyesters upon rehydration in aqueous solution. Similar to what was previously reported for poly(4a2h), poly(Malic) did not form droplets upon aqueous rehydration, likely due to the high solubility of the poly(Malic) polymers. Rehydration of poly(PA), poly(Malic-PA) and poly(4a2h-PA) resulted in turbid solutions (Figure S2, Supporting Information) composed of spherical microdroplets of size from a few micrometers up to tens of micrometers in diameter (Figure 2). Thus, we showed successful droplet assembly with three different polyester systems: a neutral polyester poly(PA), an anionic residue-containing polyester poly(Malic-PA) and a cationic residue-containing polyester poly(4a2h-PA). These three systems are sufficiently different in charge and will be used to probe potential salt–polyester interactions, which may depend

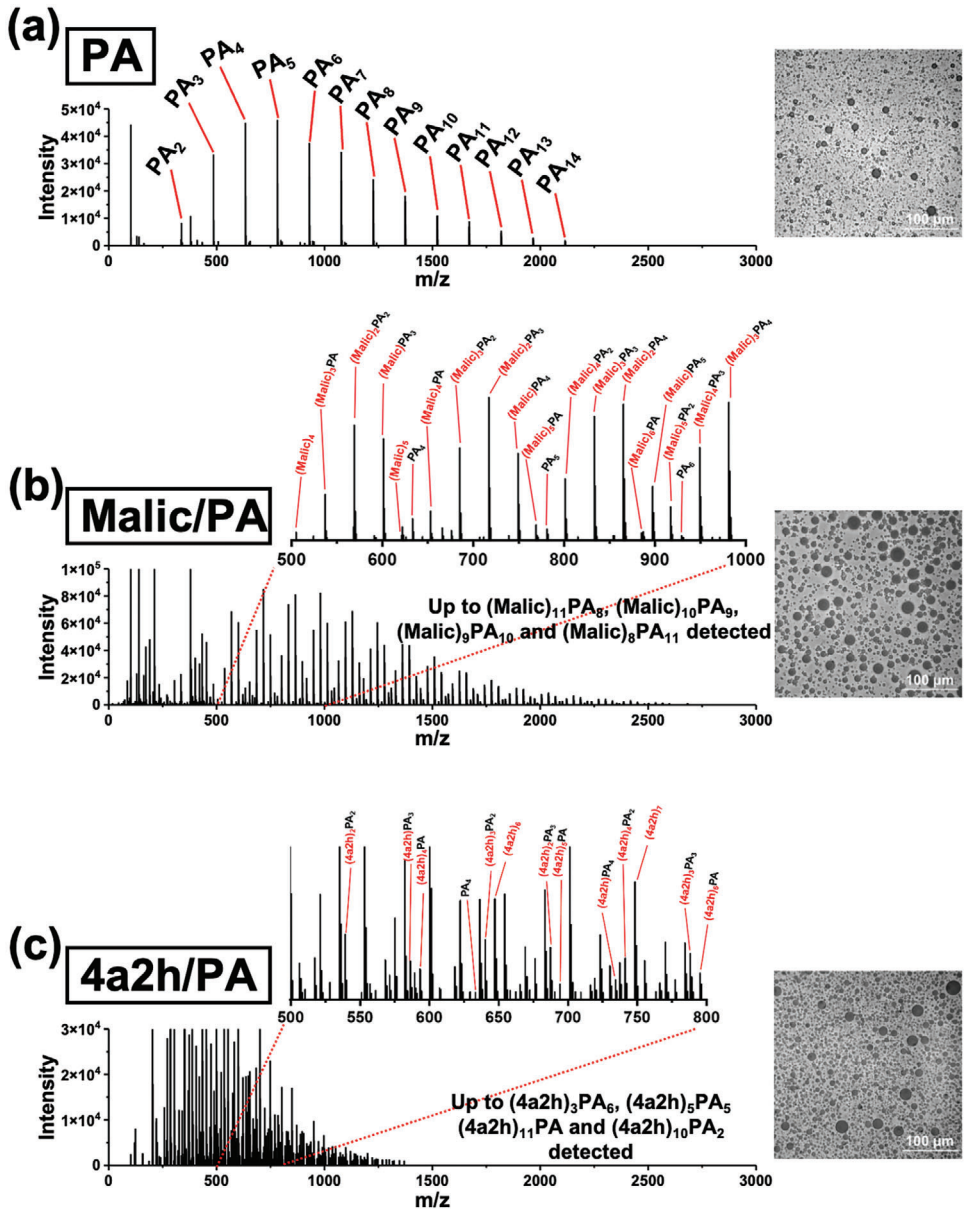

Figure 2. Representative MALDI-TOF-MS spectra showing synthesis and αHA incorporation for a) poly(PA), b) poly(Malic-PA) and c) poly(4a2h-PA). Zoom-in region insets for (b) and (c) are included for ease of visualization of the product compositions and Malic and 4a2h incorporation, respectively. Peak lists can be found in Tables S2–S4 (Supporting Information). Images showing spherical microdroplets formed from poly(PA), poly(Malic-PA), and poly(4a2h-PA) condensed phases in aqueous media visualized by optical microscopy are also included. Scale bars are 100 µm.

on electrostatic interactions. We also note that the observation of poly(Malic-PA) microdroplets is the first demonstration of primitive polymerization and assembly of acidic residue-containing polyester microdroplets. Similar to the 4a2h/PA system, we expect that increasing the Malic/PA monomer ratio prior to dehydration synthesis would also result in increased solubility and a subsequent decrease in droplet assembly propensity.

Up to 100×10^{-3} M NaCl, KCl and $MgCl_2$, and up to 10×10^{-3} M $CaCl_2$ did not appear to inhibit polyester polymerization or microdroplet assembly (Figures S3 and S4, Supporting Information). While even further increases in salt concentration (in the hundreds of millimolar range for NaCl in the early Ocean, for example[46]) or presence of other salts could affect polyester polymerization or droplet assembly, it is out of the scope of this study to probe these boundaries. Thus, subsequent experiments in this study probed individual salt concentrations only up to 100×10^{-3} M.

We next set out to investigate changes in structure or coalescence of poly(PA), poly(Malic-PA) and poly(4a2h-PA) droplets induced by the four chloride salts. None of the three droplet systems completely dissolved or disassembled upon incubation with 100×10^{-3} M of each salt (Figure S5, Supporting Information). This suggests that the droplets are kinetically trapped, rather than equilibrium structures; addition of 100×10^{-3} M $CaCl_2$ to

preformed droplets did not result in disassembly, whereas dehydration/rehydration of αHAs with 100×10^{-3} M $CaCl_2$ did not lead to droplet formation. However, the number of droplets qualitatively appears to have decreased upon salt addition. This observation matches previous observations of salt-induced polyester droplet coalescence, which would theoretically decrease the number of droplets, but simultaneously increase the average droplet size.[12] These changes in droplet properties were likely due to the salts themselves, rather than by the dilution process incurred when salt solutions are added to the polyesters, as dilution in pure water does not qualitatively appear to change the number of droplets present (Figure S6, Supporting Information).

2.2. Salt-Induced Changes in Polyester Microdroplet Number, Size, and Surface Potential

Since the glass substrates used for microscopy can affect droplet coalescence and introduce artifacts for quantification of droplet properties, we sought to use turbidimetry for quantitative droplet analysis. Assuming that a decrease in turbidity from droplets spontaneously decreasing in size is not possible, we use optical density at 600 nm as a proxy for droplet density within a solution. We first tracked the turbidity of the assembled droplets over two hours (to minimize the possibility of polyester hydrolysis and droplet disassembly at very long timescales[12]) in the presence or absence of salts.

In the absence of salts, the turbidity of poly(PA) microdroplets decreases slightly over two hours, whereas the turbidity of poly(Malic-PA) and poly(4a2h-PA) microdroplets decreases in a more pronounced manner over the same two hours (Figure S7, Supporting Information). This suggests that while there is some decrease in droplet density over time (perhaps due to coalescence or sedimentation), droplets are still relatively stable over two hours. However, poly(Malic-PA) and poly(4a2h-PA) droplets appear to decrease in number more rapidly compared to poly(PA) droplets. This could be due either to increased coalescence, or increased solubility of poly(Malic-PA) and poly(4a2h-PA) droplets. Indeed, incorporation of hydrophilic Malic or 4a2h into neutral, apolar PA-containing polyesters could lead to greater droplet solubility via weakening of noncovalent interactions, such as the hydrophobic effect, the likely main driving forces for microdroplet assembly.[12,13] Alternatively, polyesters with some hydrophilic αHAs could modulate the surface charge of the droplets, resulting in changes to colloidal stability (which will be discussed later in this study).

We observed that for poly(PA), addition of up to 10×10^{-3} M NaCl or KCl or up to 1×10^{-3} M $MgCl_2$ or $CaCl_2$ did not affect droplet density. However, incubation of poly(PA) with 100×10^{-3} M NaCl or KCl or with $\geq 10 \times 10^{-3}$ M $MgCl_2$ or $CaCl_2$, resulted in a rapid decrease in turbidity (**Figure 3**a). We observed similar trends upon incubation of poly(Malic-PA) and poly(4a2h-PA) with the salts. However, poly(Malic-PA) showed some sensitivity to the monovalent salts as low as 10×10^{-3} M and to the divalent salts as low as 1×10^{-3} M, while poly(4a2h-PA) is sensitive to 10×10^{-3} M NaCl, but not KCl (Figure S8, Supporting Information). These observations suggest that higher concentrations of and higher valence salts result in greater decreases in droplet number over time.

We thus sought to confirm whether the decrease in droplet number upon salt addition was due to coalescence by performing time-dependent dynamic light scattering (DLS) assays, enabling direct measurement of particle size as a proxy of droplet coalescence. We observed that in the absence of salts, droplet size increased only slightly, suggesting that little coalescence occurs in the absence of salts (Figure S9, Supporting Information). Upon addition of the salts, higher concentrations of salts generally resulted in greater increases in droplet size (indicating coalescence) over time. For example, 100×10^{-3} M NaCl generally resulted in more rapid coalescence than 10×10^{-3} M NaCl (Figure 3b; Figure S10, Supporting Information). Similarly, divalent salts typically required lower concentrations to effect droplet coalescence as compared to monovalent salts. For example, 100×10^{-3} M NaCl was required to drive poly(PA) coalescence, while only 10×10^{-3} M $MgCl_2$ resulted in a similar result (Figure 3b). We note that this observation does not strictly follow the Schulze-Hardy rule in DLVO theory,[47] which simplistically suggests that a divalent salt with a 64-fold lower concentration than that of a monovalent salt would induce the same result for a colloidal system. Specifically, although 100×10^{-3} M NaCl resulted in poly(PA) coalescence, 10×10^{-3} M $MgCl_2$ was required to effect the same result. However, the Schulze-Hardy rule suggests that only 1.56×10^{-3} M $MgCl_2$ would have been required. We also note exceptions in poly(Malic-PA), where 10×10^{-3} M NaCl could drive coalescence, while $CaCl_2$ required concentrations greater than 10×10^{-3} M to drive coalescence (Figure S10, Supporting Information). These discrepancies between experimental results and theoretical predictions point to the fact that polyester droplets are likely not colloids.

We next compared the trends in the changes in polyester droplet number and size upon salt addition, and deduced that decreases in droplet number (Figure 3a; Figure S8, Supporting Information) were likely due to salt-induced coalescence (Figure 3b; Figure S10, Supporting Information). While it is possible that droplet swelling due to salt uptake led to an increase in droplet size, the fact that a concurrent decrease in droplet number occurred leads us to believe that the main driver of droplet growth is coalescence. We thus hypothesized that the mechanism of salt-induced droplet coalescence may be due to modulation of droplet surface charge by uptaken salts, which could result in greater ease of interfacial interactions leading to coalescence. Thus, we sought to measure salt-induced changes in the surface potential of microdroplets. We observed through zeta-potential measurements that the surface charge in the absence of salts for all three droplet systems was slightly negative, with the poly(PA) droplet surface retaining more negative charge than poly(4a2h-PA) and poly(Malic-PA) droplet surfaces (Figure 3c; Figure S11, Supporting Information). Negatively charged droplet surfaces would lead to repulsion between droplets rather than coalescence. The negative surface charge is potentially due to accumulation of hydroxide ions at the droplet surface. Low pH systems (our system is around pH 3) lead to existence of free hydroxide ions, which appear to have some affinity to droplet or phase-separated boundaries of apolar assemblies.[48] There may also be some contribution from potential negative charges on the terminal carboxyl groups of product polyesters, which can be negatively charged depending on the ambient pH. For example, the pK_a of the PA carboxyl group is 3.46,[49] and a pH of ≈3 results in ≈25% of the

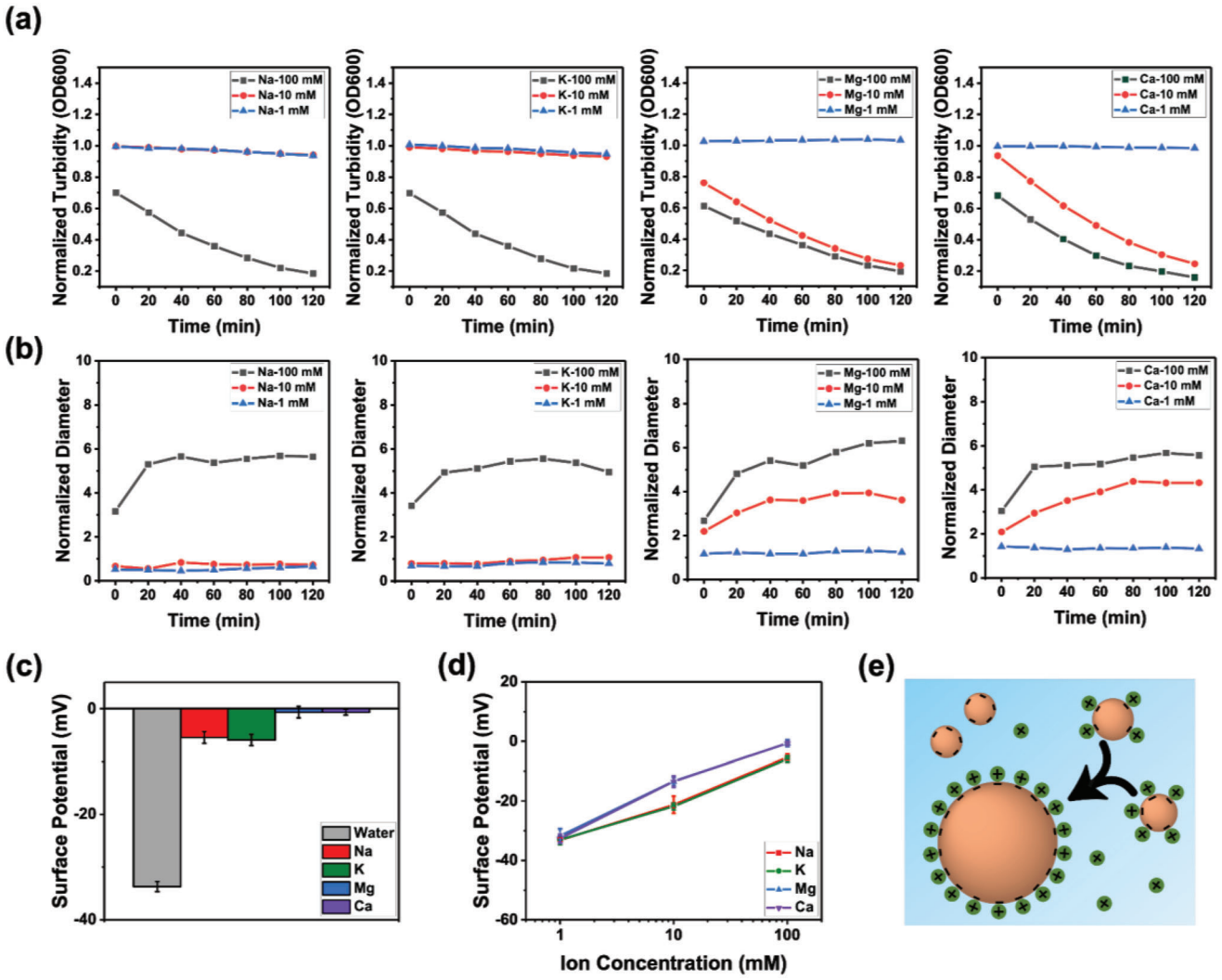

Figure 3. a) Normalized turbidity (OD600) and b) normalized particle size (DLS) was measured over 2 h for poly(PA) microdroplets in the presence of chloride salt solutions (NaCl, KCl, $MgCl_2$, and $CaCl_2$ ranging from 1, 10, to 100×10^{-3} M). Both turbidity and particle size at each time point were normalized to the initial average value before incubation (time = 0), respectively, for poly(PA) microdroplets mixed with the appropriate volume of water. c) Average and standard deviation of the surface potential of poly(PA) microdroplets in the presence of water or 100×10^{-3} M of the four chloride salt solutions. d) Relationship between the average and standard deviation of the surface potential of poly(PA) microdroplets upon incubation with the four chloride salt solutions at concentrations up to 100×10^{-3} M. e) Schematic diagram for salt-driven polyester microdroplet coalescence. $n = 3$ for OD600 and DLS experiments; $n = 6$ for surface potential experiment reported herein. Error bars indicate standard deviation.

terminal carboxyl of the product polyesters being deprotonated and retaining a negative charge. Alternatively, previous studies suggest ≈15%–20% unreacted αHA monomer remains after the synthesis reaction, some of which could also retain a negative charge.[20] Some unreacted, deprotonated monomers could also be present at the droplet surfaces.

We attribute the slightly weaker negative surface charge of poly(4a2h-PA) and poly(Malic-PA) droplets to the fact that their interiors may be less apolar than poly(PA) droplets, due to incorporation of basic or acidic residues. This could result in a greater propensity for free hydroxide anions to reside within the less apolar droplet interior, as opposed to the droplet surface, thus decreasing accumulation of negative surface charge.[48] Poly(4a2h-PA) droplets may also have protonated amino groups within incorporated 4a2h residues, contributing to even more neutralization of its surface charge compared to poly(PA).

We then observed that addition of 100×10^{-3} M of each of the four chloride salts resulted in significant neutralization of the surface charge of all polyester droplet systems, in some cases reaching nearly 0 mV (Figure 3c; Figure S11, Supporting Information). The droplet surface charge neutralization also scaled with increasing salt concentrations (Figure 3d; Figure S12, Supporting Information). We surmise that the salt-induced neutralization of droplet surface charge led to less electrostatic repulsion of the originally negatively charged droplet surfaces, which is what drives polyester microdroplet coalescence (Figure 3e).

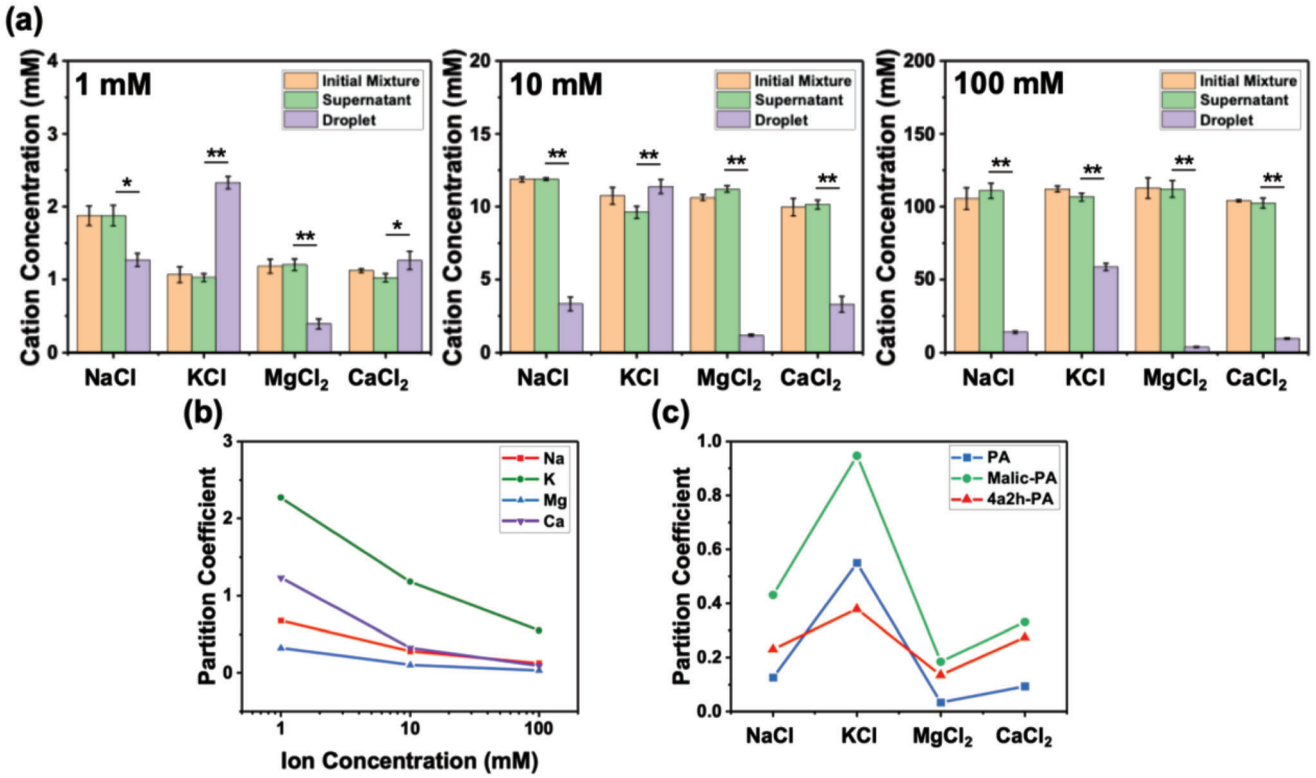

Figure 4. a) ICP-MS measurement of salt cation concentration (Na^+, K^+, Mg^{2+}, and Ca^{2+}) following incubation of poly(PA) droplets with different concentrations of the salt solutions indicated inside ("Droplet") and outside ("Supernatant") of the droplet. "Initial Mixture" indicates the sample before separation of the droplet and supernatant. In the sample with 1×10^{-3} M NaCl added, the initial Na^+ concentration was greater than 1×10^{-3} M due to detected Na^+ contaminants in the PA starting materials (Table S13, Supporting Information). *$p < 0.05$; **$p < 0.01$ (see Table S14 in the Supporting Information for relevant p-values). b) Partition coefficient of poly(PA) homopolyester microdroplets for all salt cations at concentrations up to 100×10^{-3} M. c) Partition coefficient of poly(PA), poly(Malic-PA) and poly(4a2h-PA) microdroplets for all salt cations at 100×10^{-3} M. $n = 3$ for all experiments reported herein. Error bars indicate standard deviation.

2.3. Salt Ion Uptake by Polyester Microdroplets

We next sought to quantitatively measure the amount of each salt uptaken by the polyester microdroplets by applying ICP-MS analysis to the droplets. ICP-MS is commonly used for element-specific detection and quantification, especially in geochemistry and planetary science,[50,51] and can measure salt ion concentration within the droplets following uptake. ICP-MS analysis was able to detect each of the four cations of the chloride salts (Na^+, K^+, Mg^{2+} and Ca^{2+}), but could not detect chloride anions due to poor ion formation efficiency of Cl^- in the argon plasma and isobaric interference.[52] Thus, we focused only on quantification of cation uptake. We first measured the ambient cation content in the αHA monomer solutions and polyester microdroplets in the absence of salts, and found that Na^+ was generally present at higher initial amounts compared to the other three ions in all systems other than pure 4a2h (Table S13, Supporting Information). We suspect this to be due to minor NaCl or sodiated monomer counterion impurities in the original commercially available PA and Malic monomer samples. However, we reckoned that the small scale of these impurities (Table S13, Supporting Information) would not significantly affect any of the physical effects observed and thus proceeded without removal of Na^+ impurities.

We then mixed fresh poly(PA) homopolyester microdroplets with each of the four salts at concentrations up to 100×10^{-3} M, followed by centrifugation to separate the droplets from the surrounding solution ("supernatant"). After ICP-MS analysis, we found that in all cases, the concentrations of the cations in the supernatants are nearly identical to that measured in the initial mixtures before droplet/supernatant separation (**Figure 4**a). This is likely due to the fact that the volume occupied by the droplets is small compared to the supernatant. Even if there is a large amount of salt uptaken by the droplets, the overall concentration of salt cations in the supernatant will not change significantly. We also detected each cation within the poly(PA) droplets, suggesting that the poly(PA) droplets can uptake each salt cation to some degree (Figure 4a). For all cases, the salt cation concentration in the droplets was significantly different compared to in the supernatant (Figure 4a). This suggests that the salt uptake process is likely selective and differential rather than nonselective, as would have been the case if the salt cation concentration inside and outside of the droplets was equivalent. As the droplets were incubated with salt overnight, we also believe that the measurements here are likely at equilibrium, and that the data indicate selective salt uptake rather than reflecting incomplete salt uptake due to differences in salt uptake rates.

Upon closer examination, K^+ was generally uptaken by the droplets the most, with Mg^{2+} uptaken the least. Furthermore, the relative amount of cations in solution uptaken was greater at lower salt concentrations (Figure 4a). At 1×10^{-3} M, we observed that K^+ could in fact be concentrated within poly(PA) droplets. To visualize the ability of the droplets to uptake salts differentially more clearly, we define a term called partition coefficient, which is the ratio of the cation concentration inside of the droplets versus the supernatant. A higher partition coefficient suggests greater salt uptake. A partition coefficient >1 also reflects the ability of the droplet to concentrate the uptaken salt from solution. We observe that for all cations, increasing solution concentration resulted in a decrease of the partition coefficient in poly(PA) (Figure 4b). This suggested that the droplets may have some upper limit for salt cation uptake, whether due to some physical or chemical limitation. Even increasing the total amount of salt in solution may not allow the droplets to uptake more cations than this upper limit. However, this upper limit may be different for each cation, and we may not have reached the limit in this study.

Poly(PA) microdroplets appear to differentially uptake salt cations in the following order of decreasing affinity: ($K^+ > Ca^{2+} > Na^+ > Mg^{2+}$) (Figure 4b). The exact mechanism of this difference is not clear, and may be due to a number of factors such as differences in cation structure, size[53] and/or binding affinity with poly(PA). However, the order of decreasing affinity of cation uptake matches roughly with the order of decreasing ionic radius ($K^+ > Ca^{2+} = Na^+ > Mg^{2+}$). If we consider just the divalent cations, Mg^{2+} has a larger hydration sphere than Ca^{2+}.[54] A larger hydration sphere could weaken the electrostatic interaction of the cation interior with the negatively charged polyester microdroplet surface, resulting in lower Mg^{2+} uptake compared to Ca^{2+}. For the monovalent cations, Na^+ has a larger hydration sphere than K^+, which could result in greater K^+ uptake compared to Na^+.

There may also be prebiotic evolutionary advantages for polyester droplets to selectively incorporate of K^+ over other salts, such as for generation or maintenance of protocell boundary chemical potential. We make this conjecture considering that intracellular K^+ concentration is much higher than that of Na^+, Mg^{2+} and Ca^{2+} in plant and animal cells, likely due to the action of potassium channels or the potassium-sodium pump, respectively. For instance, plants maintain a high ($100–200 \times 10^{-3}$ M) K^+ and a low ($1–10 \times 10^{-3}$ M) Na^+ concentration in their cytosol.[55] Animals also maintain a high $\approx 150 \times 10^{-3}$ M K^+ and a low $\approx 15 \times 10^{-3}$ M Na^+ concentration.[56] However, the ancient ocean likely contained much more Na^+ than K^+,[57] with some estimates suggesting up to 1100×10^{-3} M Na^+.[58] Polyester microdroplets in ancient oceans could selectively uptake low-abundance K^+, while simultaneously excluding high-abundance Na^+. This may have been one mechanism to achieve a local protocellular microenvironment containing a K^+/Na^+ ratio more on par with that observed in modern biology.

Salt–polyester interactions could be one driver for salt uptake, and polyester droplets with acidic or basic residues could lead to differences in salt uptake. We thus subjected poly(Malic-PA) and poly(4a2h-PA) microdroplets incubated with 100×10^{-3} M salt solutions to ICP-MS analysis to measure salt cation uptake. In nearly all cases, poly(Malic-PA) and poly(4a2h-PA) droplets appeared to uptake more of all cations than poly(PA) droplets (Figure S13 and Table S14, Supporting Information). We attribute these observations to the fact that incorporation of 4a2h and Malic into an otherwise neutral polymer may increase the internal polarity of the droplets, allowing ions to have more affinity to the droplets. Based on partition coefficient analysis, the order of salt cation uptake affinity was also similar for all systems (Figure 4c and Table S14, Supporting Information).

Surface charge measurements (Figure 3c,d; Figures S11 and S12, Supporting Information) suggested that incubation with 100×10^{-3} M of each salt nearly neutralized the surface charge of all droplets. However, the ICP-MS studies suggest that only a small portion of the cations in solution are uptaken by the droplets in some cases. We speculate that the cations may preferentially localize to the droplet surface, rather than being evenly distributed throughout the entire droplet. Thus, only a small concentration of salt needs to be uptaken by the droplet to completely neutralize the surface charge. This could be due to the hydrophilic character of the uptaken cations, having affinity for aqueous solution over the interior of the apolar droplets.[12,13] However, the interior of the droplets cannot be fully anhydrous, and so some salts should still reside within the droplet interior, albeit possibly at lower concentrations than at the surface. Indeed, microRaman analysis was able to detect the presence of water and ester bonds within the polyester droplets (Figures S14 and S15, Supporting Information). However, the apparent relative amount of water within the droplets appeared to be less than that the surrounding solution, reflecting the apolar nature of the droplet interior (Figures S14 and S15, Supporting Information). The addition of salts also did not significantly affect the water signal intensity within the droplets (Figures S14 and S15, Supporting Information). This suggests that while there is still some water within the droplets, the fairly apolar character of the droplet interior is still dominant even in the presence of salts.

3. Conclusion

In this work, we applied existing spectroscopic and biophysical methods to perform novel physical characterization of the salt-mediated dynamic phase behavior of polyester microdroplets. We found that polyester microdroplets can be assembled from systems that incorporate αHAs with acidic functional groups (i.e., Malic) and from reactions that contain chloride salts (up to 100×10^{-3} M in some cases). These results further increase the breadth of the primitive chemical repertoire capable of forming polyester microdroplets. This is relevant as the early Earth may have contained a large diversity of potential ester-forming monomers, including not only αHAs, but also heterocyclic monomers which can form polyesters through ring-opening polymerization.[59] The early Earth environment may also have been diverse in salinity, ranging from pure freshwater to oceanic environments to underwater hypersaline underocean brines that could have been the cradle of eventual halophile emergence.[60,61]

Additionally, we discovered that salts could drive polyester microdroplet coalesce. We propose that the high salt concentrations encountered in the primitive marine environments mentioned above may drive polyester microdroplet coalescence through neutralization of the typically negatively charged droplet surface. This in turn weakens the electrostatic repulsive forces at the droplet surface due to potential ion localization at the surface and inhibits droplet-droplet repulsion, driving coalescence. Such salt-induced

droplet coalescence could have been one driver of primitive protocellular recombination, one mechanism by which compartmentalized replicating informational polymers could have encountered greater genetic diversity. Such a phenomenon could have been one mechanism of primitive horizontal gene transfer, while also promoting polyester compositional recombination as well. It was also previously observed that vortexing and sonication can result in division of droplets in the laboratory.[12] Cycles of salt-induced droplet coalescence interspersed with environmentally driven cell division could plausibly be achieved through turbulent waves caused by storms or fumarole-induced mixing in hot springs on early Earth. Such an environment could be conducive to chemical evolution of polyester microdroplets, whether via genetic evolution of encapsulated informational polymers or via compositional evolution of the polyesters themselves.[62]

Furthermore, ICP-MS analysis revealed that polyester microdroplets uptake salt cations in a differential manner. ICP-MS is often used for materials analysis, such as in geochemistry and planetary science, and has previously been used for analysis of associative coacervates.[63] Here, we extended this notion and analyzed dissociative membraneless polyester protocell models. We observed that uptake of only a small amount of cations could result in complete neutralization of the droplet surface charges, suggesting that uptaken salts may preferentially reside at the droplet interface. However, it is unclear whether salt uptake is driven by adsorption or absorption. Further studies relating salt uptake with droplet volume are suggested to rule out one or the other possibility. While the exact mechanism of differential salt uptake is still unclear, we speculate that it is related to the ionic radius and hydration shell size of the cations. Nevertheless, we observed that changes in the primary composition of the polyesters could be one method to modulate cation uptake into polyester droplets. This result is also related to our previous observation that polyester primary composition changes can result in acquisition of an RNA segregation ability by polyester droplets.[13] Further investigation of the mechanism and evolutionary advantages of the observed differential salt uptake will be needed to holistically understand protocell-encapsulated primitive reactions that require free ions as cofactors. For example, Mg^{2+} is essential for RNA folding, ribozyme catalysis and nonenzymatic RNA replication,[64–66] and understanding the feasibility of such processes within the polyester droplets is necessary. Similarly, whether encapsulated Mg^{2+} (or another cation) could modulate nucleic acid uptake into the droplets due to salt-nucleic acid binding, or vice versa, is also worth a detailed follow-up study in the future.

Finally, the study of the effects of different types of salt on membraneless polyester microdroplets could also be relevant to the origin and existence of potential life off of Earth. For example, aqueous environments and high salinity are relatively common in inner Solar planetary bodies (e.g., Mars)[67–70] or even the exooceans of the icy moons of the outer solar system such as Europa or Enceladus.[71,72] αHA monomers could also have been existed on Mars or the icy moons via meteoritic delivery,[7,73–74] especially on Mars, where extramartian organic delivery via meteorites has been observed.[75] Experimental demonstration of reducing chemistries simulating those of Mars or Enceladus conditions has also demonstrated the potential synthesis of αHA monomers in those environments.[76,77] Finally, evaporation of surface liquid water in the past on Mars,[78] dehydration synthesis in ice on Europa[79] or low-water activity pores on Enceladus[80–82] could provide appropriate conditions for the dehydration synthesis chemistries presented herein. Nevertheless, we do acknowledge that αHAs have not been directly detected on Mars or the icy oceans of extraterrestrial bodies, perhaps owing to instrument detection limits or preservation issues,[83–85] and thus it cannot be ruled out that αHAs exist on other extraterrestrial bodies. Thus, further development of more sensitive or novel methods to analyze and characterize αHAs, polyesters, and their subsequent microdroplets in extraterrestrial environments will be necessary to more clearly reveal the relevance of polyester-based protocell systems to the origins of life both on and off Earth.

4. Experimental Section

Chemicals: PA (DL-3-phenyllactic acid) was purchased from Sigma-Aldrich (St. Louis, MO, USA). 4a2h ((S)-(-)-4-amino-2-hydroxybutyric acid) and Malic (DL-malic acid) were purchased from Tokyo Chemical Industry Co. (Chuo-ku, Tokyo, Japan). All chloride salts (NaCl, KCl, $MgCl_2{\cdot}6H_2O$ and $CaCl_2{\cdot}2H_2O$) were purchased from Nacalai Tesque (Nakagyo-ku, Kyoto, Japan). All other chemicals, including acetonitrile, were purchased from Sigma-Aldrich.

Dehydration Synthesis of Polyesters: All syntheses were carried out in 13 mm borosilicate test tubes (Thermo Fisher Scientific, Minato-ku, Tokyo, Japan) or 1.5 mL microcentrifuge tubes (Eppendorf, Chiyoda-ku, Tokyo, Japan), starting from a total volume of 500 µL of monomer solution and a total starting monomer concentration of 500×10^{-3} M. This meant that all homopolyesters started with 500 µL of a 500×10^{-3} M stock solution, whereas heteropolyester cases (1:1 Malic/PA and 1:1 4a2h/PA) started with 250 µL each of both stock solutions at 500×10^{-3} M, i.e., 250 µL of a 500×10^{-3} M PA stock solution was mixed with a 500×10^{-3} M Malic stock solution (resulting in 250×10^{-3} M of each monomer after mixing). In addition, for polymerization in the presence of salts, 250 µL of a 500×10^{-3} M PA stock solution was mixed with 250 µL of NaCl, KCl, $MgCl_2$ or $CaCl_2$ with final salt concentrations of 10×10^{-3} or 100×10^{-3} M after mixing. All stock solutions were prepared in ultrapure water (18.2 MΩ cm and <5 ppb total organic carbon, Barnstead Smart2Pure system, Thermo Fisher Scientific) after vortexing and sonication without adjustment of pH. Stock solutions were stored at 4 °C until use. The PA stock solution did not fully solubilize without repeated heating/vortexing cycles; when preparing PA stock solution, the solution was heated to 60 °C on a heating plate with occasional vortexing to fully solubilize PA in solution, followed by cooling to room temperature.

The synthesis reactions were allowed to dry uncovered for 1 week at constant 80 °C using Sahara 310 or 320 dry heating baths (Rocker Scientific, New Taipei City, Republic of China) in a draft chamber to mimic a primitive dehydrating environment. After 1 week, the samples were completely dry and formed a gel-like state. All macroscopic condensed phase photographs were collected with a Huawei Mate 10 Pro (Shenzhen, Guangdong, China).

Matrix-Assisted Laser Desorption Ionization Time-of-Flight Mass Spectrometry (MALDI-TOF-MS): MALDI-TOF-MS was performed using an ultrafleXtreme Bruker Daltonics (Billerica, MA, USA) MALDI-TOF-MS in positive ion mode. External mass calibration was conducted using standard peptide mixtures provided by the user facility. Poly(Malic) was dissolved in water, whereas poly(PA), poly(Malic-PA) and poly(4a2h-PA) were dissolved in tetrahydrofuran (THF) (10 mg mL^{-1}). CHCA (alpha-cyano-4-hydroxy-cinnamic acid) was chosen as the sample matrix for all samples, except poly(PA) polymerized with 10 and 100×10^{-3} M $CaCl_2$ used DCTB (trans-2-[3-(4-tert-butylphenyl)-2-methyl-2-propenylidene] malononitrile) as the matrix after optimization due to poor spectral quality when CHCA was used as the matrix.

The sample matrix was first dissolved in THF. Dissolved samples were then mixed with the matrices (1:10 (v/v)) and applied to the plate before

analysis. Monoisotopic peaks were then identified by isolating the highest intensity peak in an isotope envelope corresponding to a polymer product using a peak list generated from mMass (Open Source Software, Prague, Czech Republic) to subtract the matrix background signal. Major peaks were isolated by applying the following parameters: S/N > 10, absolute peak intensity >1000 and baselining (100 precision and 0 relative offset). Mass accuracy in ppm was calculated by comparing the observed mass with the calculated mass for major peaks corresponding to polymerization products. Detailed peak lists are presented in Supporting Information; generally, only sodiated peaks (which are the most abundant and effectively demonstrate stepwise residue addition on a growing polyester polymer chain) are reported unless otherwise noted.

Droplet Formation: All synthesized polyesters were first rehydrated in 500 µL 4:1 (v/v) water:acetonitrile in the original reaction vessel without pH adjustment, followed by brief sonication and vortexing to generate turbid suspensions containing microdroplets. Similar to previous studies, acetonitrile, a potentially prebiotic solvent, was incorporated into the solvent since a pure water solvent did not result in significant microdroplet formation.[11]

Optical Microscopy: Following rehydration of the relevant polymerization products in 500 µL 4:1 (v/v) water:acetonitrile, 40 µL of the fresh droplet solution was added to 40 µL of either water or a salt stock solution (of concentration twice that of the final indicated salt concentration, i.e., 200×10^{-3} M salt stock solution was added for samples with a final indicated salt concentration of 100×10^{-3} M), to achieve a final mixture of the indicated salt concentration. Then, 3.5 µL of each mixed salt-droplet sample was applied to a slide glass (76 × 26 × 1 mm, Matsunami Glass, Kishiwada-shi, Osaka, Japan) into a vacated area within a double-sided tape ring, produced by punching a hole through strong-type double-sided tape (Naisutakku, Nichiban KK, Tokyo, Japan). This was then covered by a second glass coverslip (No. 1 18 × 18 mm, Matsunami Glass) to prevent evaporation. Optical microscopy images were acquired with a DM5500 B upright epifluorescence microscope (HC PL FLUOTAR 40×/0.80 PH2 air objective, Leica, Wetzlar, Germany) with the Leica LAS X software and analyzed using FIJI (Fiji is Just ImageJ, http://fiji.sc).

Turbidity Measurements: Following rehydration of the relevant polymerization products in 500 µL 4:1 (v/v) water:acetonitrile, 40 µL of the fresh droplet solution was added to 40 µL of either water or a salt stock solution to achieve a final mixture of the indicated salt concentration. Then, 40 µL of each mixed salt-droplet sample was pipetted into a separate well of a 384-well glass-bottom plate (Corning 4581, USA). Optical density at 600 nm was then measured using a Multimode Plate Reader (Enspire 2300 Multilabel reader, PerkinElmer, Singapore) at a controlled temperature of 25 °C, with 5 s orbital shaking at 200 rpm. The turbidity was recorded for a period of 2 h over 6 acquisitions (20 min each). Each measurement was repeated three times.

Dynamic Light Scattering Measurements: The average diameter of polyester microdroplets were determined using a DelsaMax Core dynamic light scattering (DLS) instrument (Beckman Coulter, Brea, CA, USA) equipped with a 100 mW laser (660.9 nm) and 90° detector. Following rehydration of the relevant polymerization products in 500 µL 4:1 (v/v) water:acetonitrile, 40 µL of the fresh droplet solution was added to 40 µL of either water or a salt stock solution to achieve a final mixture of the indicated salt concentration. Then, 45 µL of each mixed salt-droplet sample was separately loaded into a 45 µL quartz microcuvette, and a cap was put on top. The intensity of scattered light was recorded for a period of 2 h over six acquisitions (20 min each). Each measurement was repeated three times. The software package DelsaMax 1.0.0.23 was used to analyze the data and to calculate the mean particle size.

Zeta Potential Measurement: Zeta potential was measured using a Horiba SZ-100 Nanoparticle Analyzer (Horiba, Kyoto, Japan). Following rehydration of the relevant polymerization products in 500 µL 4:1 (v/v) water:acetonitrile, 300 µL of the fresh droplet solution was added to 300 µL of either water or a salt stock solution, to achieve a final mixture of the indicated salt concentration. 300 µL of the mixture was then transferred to the appropriate sample cuvette, and analyzed on the instrument. The test temperature was set at 25 °C. Each measurement was repeated six times.

Inductively Coupled Plasma Mass Spectrometry: ICP-MS analyses were performed with He gas in kinetic energy discrimination mode using a single quadrupole (SQ-KED mode). A microflow PFA nebulizer (PFA-20, ESI, USA) was used with a self-aspiration system. The sample uptake time was set to 80 s, of which the actual integration time is 50 s. The dwell time of each target ion (Na^+, K^+, Mg^{2+} and Ca^{2+}) is 0.01 s. The analytical method contains 19 isotopes of 15 elements, including the target elements. The calibration curve method was applied to determine ion concentrations. As a standard solution for analysis, a mixture of the same salt solution used for incubation was measured once for every two samples as a standard material. This standard was prepared by mixing 1 mL each of 20×10^{-3} M salt solutions of Na^+ and K^+ and 200×10^{-3} M salt solutions of Mg^{2+} and Ca^{2+}, and diluting 10 times twice with 0.5 M HNO_3, which was prepared with distilled nitric acid (EL grade 69%, Kanto Chemicals) and USQ water (further deionized Milli-Q water), to a final concentration of 0.05×10^{-3} M for Na^+ and K^+ and 0.5×10^{-3} M for Mg^{2+} and Ca^{2+}. The concentrations of standard solutions and samples ("initial mixture," "supernatant," and "droplets") for ICP-MS analysis were adjusted so that all ions were detected by the same detector (sample details are described below).

For "initial mixture" samples (without separation of droplets from supernatant), poly(PA) homopolyester microdroplet solutions were first prepared by dissolving the reaction products in Eppendorf tube in 500 µL 4:1 (v/v) water:acetonitrile, followed by brief sonication and vortexing. Then, an equivalent volume of water or chloride salt solutions (NaCl, KCl, $MgCl_2$, and $CaCl_2$) to final salt concentrations of 1, 10, or 100×10^{-3} M was added to the droplet mixture, followed by vortexing. Then, 200 µL of each sample was pipetted into different polypropylene bottles (8 mL size, Thermo Scientific Nalgene) respectively for further sample processing. Each sample mixture was then diluted by a different factor to match the detection/sensitivity of the instrument. For "initial mixture" sample mixtures containing only water, 1×10^{-3} M NaCl, 1×10^{-3} M KCl, 10×10^{-3} M $MgCl_2$ and 10×10^{-3} M $CaCl_2$ a 3800 µL of 0.5 M HNO_3 solution was added into each respective sample bottle to reach a final dilution factor of 20. For "initial mixture" sample mixtures containing 10×10^{-3} M NaCl, 10×10^{-3} M KCl, 100×10^{-3} M $MgCl_2$ and 100×10^{-3} M $CaCl_2$, 7800 µL of 0.5 M HNO_3 solution was added to each respective sample bottle; then, 200 µL of the diluted mixtures with HNO_3 were further diluted with 800 µL of 0.5 M HNO_3 solution so that the final dilution factor became 200. For "initial mixture" sample mixtures containing 100×10^{-3} M NaCl and 100×10^{-3} M KCl, 7800 µL of 0.5 M HNO_3 solution was initially added to each respective sample bottle; then, 200 µL of the diluted mixtures with HNO_3 were further diluted with 9800 µL 0.5 M HNO_3 solution, so that the final dilution factor became 2000. Finally, for the "initial mixture" sample mixtures containing 1×10^{-3} M $MgCl_2$ and 1×10^{-3} M $CaCl_2$, 800 µL of 0.5 M HNO_3 solution was added to each respective sample bottle to reach a final dilution factor of 5. In all cases, 1 mL of each "initial mixture" sample solution was prepared for further analysis by ICP-MS.

Meanwhile, "supernatant" and "droplet" solutions were prepared in the following way. After removing 200 µL as an "initial mixture" aliquot, the remaining sample (800 µL) was incubated overnight and centrifuged (HITACHI High-Speed Micro Centrifuge model CF16RN himac, Tokyo, Japan) at 5000 rpm for 15 min at 23 °C; the droplets accreted to the bottom of the Eppendorf tube. The supernatants were subsequently separated from the droplets by pipette. Then, for "supernatant" sample mixtures with water (no salts added), 1×10^{-3} M NaCl and 1×10^{-3} M KCl, 780 µL of each supernatant solution was first diluted with 7020 µL of 0.5 M HNO_3 solution; then, 500 µL of the diluted mixtures with HNO_3 were further diluted with 500 µL of 0.5 M HNO_3 solution so that the final dilution factor became 20. For "supernatant" sample mixtures containing 10×10^{-3} M $MgCl_2$ and 10×10^{-3} M $CaCl_2$, 500 µL of each supernatant solution was first diluted with 9500 µL of 0.5 M HNO_3 solutions so that the final dilution factor became 20. For "supernatant" sample mixtures containing 10×10^{-3} M NaCl and 10×10^{-3} M KCl, 780 µL of each supernatant solution was first diluted with 7020 µL of 0.5 M HNO_3 solution; then, 200 µL of the diluted mixtures with HNO_3 were further diluted with 3800 µL of 0.5 M HNO_3 solution so that the final dilution factor became 200. For "supernatant" sample mixtures containing 100×10^{-3} M $MgCl_2$ and 100×10^{-3} M $CaCl_2$, 500 µL of

each supernatant solution was first diluted with 4500 µL of 0.5 M HNO_3 solution; then, 200 µL of the diluted mixtures with HNO_3 were further diluted with 3800 µL of 0.5 M HNO_3 solution so that the final dilution factor became 200. For "supernatant" sample mixtures containing 100×10^{-3} M NaCl and 100×10^{-3} M KCl, 780 µL of each supernatant solution was first diluted with 7020 µL of 0.5 M HNO_3 solution; then, 200 µL of the diluted mixtures with HNO_3 were further diluted with 9800 µL of 0.5 M HNO_3 solution; finally, 250 µL of the twice-diluted mixtures with HNO_3 were again diluted with 750 µL of 0.5 M HNO_3 solution so the final dilution factor became 2000. For "supernatant" sample mixtures containing 1×10^{-3} M $MgCl_2$ and 1×10^{-3} M $CaCl_2$, 500 µL of each supernatant solution was diluted with 2000 µL of 0.5 M HNO_3 solution so that the final dilution factor became 5. In all cases, 1 mL of each "supernatant" sample solution was prepared for further analysis by ICP-MS.

For the remaining accreted droplets after removal of supernatant, 15 µL of each sample was first dissolved in 100 µL acetonitrile. For "droplet" samples containing water and 1×10^{-3} M NaCl, KCl, $MgCl_2$ or $CaCl_2$, 500 µL of 0.5 M HNO_3 solution was added to each acetonitrile-dissolved sample so that the final dilution factor became 41. For "droplet" samples containing 10×10^{-3} M NaCl, KCl, $MgCl_2$ or $CaCl_2$, 900 µL of 0.5 M HNO_3 solution was first added to each acetonitrile-dissolved sample; then, 100 µL of the HNO_3-diluted mixtures were further diluted with 900 µL of 0.5 M HNO_3 solution so that the final dilution factor became 677. Finally, 1 mL of each "droplet" sample solution was prepared for further analysis by ICP-MS.

For poly(Malic-PA) and poly(4a2h-PA) heteropolyester microdroplets in the presence of 100×10^{-3} M of each of the four chloride salt solutions, the preparation steps for ICP-MS measurements on "initial mixture" and "supernatant" samples were identical to the preparation of the poly(PA) homopolyester samples above. For the "droplet" sample solutions, 10 µL of each sample was first dissolved in 100 µL acetonitrile and then prepared using the same steps as for poly(PA) homopolyester samples for further analysis by ICP-MS.

For blank determination of monomers, 500×10^{-3} M pure PA, Malic and 4a2h were prepared after weighing the powder and dissolution in 10 mL USQ water. Each monomer solution was diluted with 1 M HNO_3 solution at a 1 to 1 volume ratio (1:1 v/v), and then subjected directly to analysis by ICP-MS.

All "initial mixture" and "supernatant" samples were measured in triplicate (separate experiments) and all "droplet" samples were measured in triplicate, but each of the three experiments included two technical replicates (for a total of six acquisitions for each "droplet" sample); the technical replicates were first averaged to obtain the measured cation value for each experimental run, and the averaged values for each of the three experimental replicates were used for further analysis.

MicroRaman Spectroscopy: A laser Raman microspectrometer (RAMANtouch, nanophoton, Osaka, Japan) was used to measure the Raman spectrum of one region of interest inside and one region of interest outside one individual polyester microdroplet (roughly 10 µm in diameter) under an objective lens. 40 µL of each indicated polyester microdroplet solution (after dilution in 500 µL 4:1 (v/v) water:acetonitrile) and 40 µL of water or respective salt solution (for a final salt concentration of 100×10^{-3} M) were freshly mixed, followed by centrifugation (15 000 rpm for 1 min at 23 °C; Model 3780; Kubota Co., Tokyo, Japan). Following the same preparation process in optical microscopy observations, 3.5 µL of the polyester solutions were pipetted into the vacated area covered by a second glass coverslip to prevent evaporation and then subjected to microRaman analysis. The excitation laser was a green laser with a wavelength of 532 nm. Each Raman spectrum was obtained with 60 s exposure time and no accumulation. The excitation power was roughly 11 mW during sample measurement. Confocal experiments were carried out with a pinhole aperture of 50 µm. The measurement spot size was about 2 µm using an objective lens (Nikon, 20X, NA 0.45). Measurements were made at three different locations inside and outside the same individual droplet and average values were calculated.

Statistical Analysis: 1) Preprocessing of data was performed for MALDI-MS spectra as described above. Other data were not preprocessed. 2) All relevant data are presented as mean, with error bars indicating standard deviation. 3) Sample size for each analysis is indicated as described above. 4) Statistical differences between two sets of parallel data were carried out with comparisons via a two-tailed paired *t*-test. Statistically significant differences were designated as *p*-values <0.01. Statistically significant differences are indicated by $*p < 0.05$; $**p < 0.01$. 5) All statistical *t*-test analyses were performed by Microsoft Excel for Mac (version 16.71). All statistical curves were plotted under Origin 2022 (64-bit) SR1.

Supporting Information

Supporting Information is available from the Wiley Online Library or from the author.

Acknowledgements

Experiments at the Okayama University Institute of Planetary Materials (IPM) performed by C.C., C.S., T.K., K.K., E.N., C.P. and T.Z.J. were supported by a joint research program carried out at the Institute for Planetary Materials, Okayama University, supported by "Joint Usage/Research Center" program by MEXT, Japan, to C.C., R.A., R.Y., T.Z.J., T.K., E.N., K.K., and C.P. R.Y., is further supported by Japan Society for the Promotion of Science (JSPS) Grant-in-aid 21K14029. The work of A.A. is supported by the Science and Technology Development Fund, Macau SAR, China (File no. SKL-LPS(MUST)-2021-2023) and by the Macau University of Science and Technology Faculty Research Grant (Project Grant No. FRG-22-079-LPS). A.W. is supported by an Australian Research Council Discovery Early Career Award DE210100291. K.C. is supported by the Research Encouragement Grant (GGPM-2021-057) by the National University of Malaysia and Visitor Grant (ZF-2022-008). J.H. is supported by Pioneer Hundred Talents Program of Chinese Academy of Sciences and CIFAR Azrieli Global Scholarship. T.Z.J. is further supported by JSPS Grants-in-aid 18K14354 and 21K14746, a Tokyo Institute of Technology Yoshinori Ohsumi Fund for Fundamental Research, a Start-up Grant from the Earth-Life Science Institute (ELSI), the Mizuho Foundation for the Promotion of Sciences and by the Assistant Staffing Program by the Gender Equality Section, Diversity Promotion Office, Tokyo Institute of Technology. C.C., R.Y., R.A., and T.Z.J. are members of ELSI of the Tokyo Institute of Technology, which is sponsored by a grant from the Japan Ministry of Education, Culture, Sports, Science and Technology as part of the World Premier International Research Center Initiative. The authors thank M. Koizumi (The Titech Materials Analysis Division) for assistance with MALDI, Y. Nakazono (Division of Platform for Analytical Instrument at Titech) for assistance with surface potential measurement, and K. Tanaka (PML Lab, IPM, Okayama University at Misasa) for assistance with ICP-MS experiments.

Conflict of Interest

The authors declare no conflict of interest.

Author Contributions

C.C. and T.Z.J. conceived the research. C.C. and T.Z.J. designed the experiments with helpful discussions with all other authors. C.C. and R.A. performed the polyester synthesis and optical image observations; C.C. performed MALDI-TOF-MS analysis under the guidance of K.C. and T.Z.J.; C.C. performed OD600, DLS and zeta-potential measurement experiments and data analysis; C.C. and M.I. performed the MicroRaman experiment and analysis; C.C. and C.S. performed the ICP-MS experiments and data analysis with the assistance of R.Y. and T.Z.J. in the clean room at the pheasant memorial laboratory (PML), Institute for Planetary Materials (IPM), Okayama University at Misasa; C.C. wrote the original draft; C.C. and T.Z.J. reviewed and edited the subsequent drafts and the final manuscript. All authors have discussed the results and commented on the paper.

Data Availability Statement

The data that support the findings of this study are available in the supplementary material of this article.

Keywords

membraneless compartments, origins of life, phase separation, prebiotic chemistry, protocells

Received: January 29, 2023
Revised: April 23, 2023
Published online: May 18, 2023

[1] N. Guttenberg, N. Virgo, K. Chandru, C. Scharf, I. Mamajanov, *Philos. Trans. R. Soc., A* **2017**, *375*, 20160347.
[2] K. Chandru, I. Mamajanov, H. J. Cleaves, T. Z. Jia, *Life* **2020**, *10*, 6.
[3] J. G. Forsythe, S. S. Yu, I. Mamajanov, M. A. Grover, R. Krishnamurthy, F. M. Fernández, N. V. Hud, *Angew. Chem., Int. Ed.* **2015**, *54*, 9871.
[4] K. Chandru, N. Guttenberg, C. Giri, Y. Hongo, C. Butch, I. Mamajanov, H. J. Cleaves, *Commun. Chem.* **2018**, *1*, 30.
[5] E. T. Parker, H. J. Cleaves, J. L. Bada, F. M. Fernández, *Rapid Commun. Mass Spectrom.* **2016**, *30*, 2043.
[6] L. M. Barge, E. Flores, M. M. Baum, D. G. V. Velde, M. J. Russell, *Proc. Natl Acad. Sci. USA* **2019**, *116*, 4828.
[7] E. T. Peltzer, J. L. Bada, *Nature* **1978**, *272*, 443.
[8] X. Zang, Y. Ueno, N. Kitadai, *Astrobiology* **2022**, *22*, 387.
[9] E. Camprubí, J. W. de Leeuw, C. H. House, F. Raulin, M. J. Russell, A. Spang, M. R. Tirumalai, F. Westall, *Space Sci. Rev.* **2019**, *215*, 56.
[10] B. Damer, D. Deamer, *Astrobiology* **2020**, *20*, 429.
[11] S. Alberti, *Curr. Biol.* **2017**, *27*, R1097.
[12] T. Z. Jia, K. Chandru, Y. Hongo, R. Afrin, T. Usui, K. Myojo, H. J. Cleaves, *Proc. Natl Acad. Sci. USA* **2019**, *116*, 15830.
[13] T. Z. Jia, N. V. Bapat, A. Verma, I. Mamajanov, H. J. Cleaves, K. Chandru, *Biomacromolecules* **2021**, *22*, 1484.
[14] J. R. Vieregg, M. Lueckheide, A. B. Marciel, L. Leon, A. J. Bologna, J. R. Rivera, M. V. Tirrell, *J. Am. Chem. Soc.* **2018**, *140*, 1632.
[15] B. S. Schuster, E. H. Reed, R. Parthasarathy, C. N. Jahnke, R. M. Caldwell, J. G. Bermudez, H. Ramage, M. C. Good, D. A. Hammer, *Nat. Commun.* **2018**, *9*, 2985.
[16] N. Martin, L. Tian, D. Spencer, A. Coutable-Pennarun, J. L. R. Anderson, S. Mann, *Angew. Chem.* **2019**, *131*, 14736.
[17] Y. Zhang, T. Kojima, G. A. Kim, M. P. McNerney, S. Takayama, M. P. Styczynski, *Nat. Commun.* **2021**, *12*, 5724.
[18] A. I. Oparin, A. E. Braunshtein, A. G. Pasynskii, *The Origin of Life on the Earth: Held at Moscow, 19–24 August 1957*, Elsevier, Amsterdam **2013**.
[19] J. B. S. Haldane, *Ration. Annu.* **1929**, *148*, 3.
[20] R. Afrin, C. Chen, D. Sarpa, M. Sithamparam, R. Yi, C. Giri, I. Mamajanov, H. J. Cleaves, K. Chandru, T. Z. Jia, *Macromol. Chem. Phys.* **2022**, *223*, 2200235.
[21] B. Ghosh, R. Bose, T. Y. D. Tang, *Curr. Opin. Colloid Interface Sci.* **2021**, *52*, 101415.
[22] R. R. Poudyal, R. M. Guth-Metzler, A. J. Veenis, E. A. Frankel, C. D. Keating, P. C. Bevilacqua, *Nat. Commun.* **2019**, *10*, 490.
[23] C. Chen, P. Li, W. Luo, Y. Nakamura, V. S. Dimo, K. Kanekura, Y. Hayamizu, *Langmuir* **2021**, *37*, 5635.
[24] C. Chen, H. Jia, Y. Nakamura, K. Kanekura, Y. Hayamizu, *ACS Omega* **2022**, *7*, 19280.
[25] E. A. Frankel, P. C. Bevilacqua, C. D. Keating, *Langmuir* **2016**, *32*, 2041.
[26] P. Li, P. Holliger, S. Tagami, *Nat. Commun.* **2022**, *13*, 3050.
[27] T. Yoshizawa, R. S. Nozawa, T. Z. Jia, T. Saio, E. Mori, *Biophys. Rev.* **2020**, *12*, 519.
[28] C. Chen, Y. Yamanaka, K. Ueda, P. Li, T. Miyagi, Y. Harada, S. Tezuka, S. Narumi, M. Sugimoto, M. Kuroda, Y. Hayamizu, K. Kanekura, *J. Cell Biol.* **2021**, *220*, e202103160.
[29] H. Nanaura, H. Kawamukai, A. Fujiwara, T. Uehara, Y. Aiba, M. Nakanishi, T. Shiota, M. Hibino, P. Wiriyasermkul, S. Kikuchi, R. Nagata, M. Matsubayashi, Y. Shinkai, T. Niwa, T. Mannen, N. Morikawa, N. Iguchi, T. Kiriyama, K. Morishima, R. Inoue, M. Sugiyama, T. Oda, N. Kodera, S. Toma-Fukai, M. Sato, H. Taguchi, S. Nagamori, O. Shoji, K. Ishimori, H. Matsumura, et al., *Nat. Commun.* **2021**, *12*, 5301.
[30] D. Deamer, *Life* **2022**, *12*, 1429.
[31] H. Cinar, Z. Fetahaj, S. Cinar, R. M. Vernon, H. S. Chan, R. H. A. Winter, *Chem. – Eur. J* **2019**, *25*, 13049.
[32] Z. Fetahaj, L. Ostermeier, H. Cinar, R. Oliva, R. Winter, *J. Am. Chem. Soc.* **2021**, *143*, 5247.
[33] G. Krainer, T. J. Welsh, J. A. Joseph, J. R. Espinosa, S. Wittmann, E. de Csilléry, A. Sridhar, Z. Toprakcioglu, G. Gudiškytė, M. A. Czekalska, W. E. Arter, J. Guillén-Boixet, T. M. Franzmann, S. Qamar, P. S. George-Hyslop, A. A. Hyman, R. Collepardo-Guevara, S. Alberti, T. P. J. Knowles, *Nat. Commun.* **2021**, *12*, 1085.
[34] M. G. F. Last, S. Deshpande, C. Dekker, *ACS Nano* **2020**, *14*, 4487.
[35] F. J. Millero, R. Feistel, D. G. Wright, T. J. McDougall, *Deep. Res. Part I Oceanogr. Res. Pap.* **2008**, *55*, 50.
[36] K. Yusenko, S. Fox, P. Guni, H. Strasdeit, *Zeit. Anorg. Allg. Chem.* **2008**, *634*, 2347.
[37] V. V. Matchkov, H. Gustafsson, A. Rahman, D. M. B. Boedtkjer, S. Gorintin, A. K. Hansen, E. V. Bouzinova, H. A. Praetorius, C. Aalkjaer, H. Nilsson, *Circ. Res.* **2007**, *100*, 1026.
[38] B. Zhang, Y. Zhang, Z. X. Wang, Y. Zheng, *J. Biol. Chem.* **2000**, *275*, 25299.
[39] S. S. Kim, L. Ma, J. Unruh, S. McKinney, C. R. Yu, *BMC Neurosci.* **2015**, *16*, 4.
[40] H. Jing, Q. Bai, Y. Lin, H. Chang, D. Yin, D. Liang, *Langmuir* **2020**, *36*, 8017.
[41] T. P. Fraccia, T. Z. Jia, *ACS Nano* **2020**, *14*, 15071.
[42] E. Spruijt, *Commun. Chem.* **2023**, *6*, 23.
[43] H. J. Cleaves, *Life* **2013**, *3*, 331.
[44] I. Mamajanov, P. J. Macdonald, J. Ying, D. M. Duncanson, G. R. Dowdy, C. A. Walker, A. E. Engelhart, F. M. Fernández, M. A. Grover, N. V. Hud, F. J. Schork, *Macromolecules* **2014**, *47*, 1334.
[45] E. P. Nardi, F. S. Evangelista, L. Tormen, T. D. SaintPierre, A. J. Curtius, S. S. d. Souza, F. Barbosa, *Food Chem.* **2009**, *112*, 727.
[46] T. Z. Jia, T. P. Fraccia, *Crystals* **2020**, *10*, 964.
[47] Y. Chu, J. Chen, F. Haso, Y. Gao, J. E. S. Szymanowski, P. C. Burns, T. Liu, *Chem. – Eur. J.* **2018**, *24*, 5479.
[48] P. Creux, J. Lachaise, A. Graciaa, J. K. Beattie, A. M. Djerdjev, *J. Phys. Chem. B* **2009**, *113*, 14146.
[49] E. Debonne, A. Vermeulen, N. Bouboutiefski, T. Ruyssen, F. Van Bockstaele, M. Eeckhout, F. Devlieghere, *Food Microbiol.* **2020**, *88*, 103407.
[50] E. Nakamura, K. Kobayashi, R. Tanaka, T. Kunihiro, H. Kitagawa, C. Potiszil, T. Ota, C. Sakaguchi, M. Yamanaka, D. M. Ratnayake, H. Tripathi, R. Kumar, M. L. Avramescu, H. Tsuchida, Y. Yachi, H. Miura, M. Abe, R. Fukai, S. Furuya, K. Hatakeda, T. Hayashi, Y. Hitomi, K. Kumagai, A. Miyazaki, A. Nakato, M. Nishimura, T. Okada, H. Soejima, S. Sugita, A. Suzuki, et al., *Proc. Japan Acad. Ser. B* **2022**, *98*, 227.
[51] E. Nakamura, T. Kunihiro, T. Ota, C. Sakaguchi, R. Tanaka, H. Kitagawa, K. Kobayashi, M. Yamanaka, Y. Shimaki, G. E. Bebout, H. Miura, T. Yamamoto, V. Malkovets, V. Grokhovsky, O. Koroleva, K. Litasov, *Proc. Japan Acad. Ser. B* **2019**, *95*, 165.
[52] J. E. Lesniewski, W. P. McMahon, K. Jorabchi, *J. Anal. At. Spectrom.* **2018**, *33*, 1981.

[53] S. Earle, *Physical Geology*, 2nd ed., BCcampus, Victoria, B.C., Canada. **2006**.
[54] P. Dalai, N. Sahai, *Trends Biochem. Sci.* **2019**, *44*, 331.
[55] H. W. Koyro, R. Stelzer, *J. Plant Physiol.* **1988**, *133*, 441.
[56] A. V. Melkikh, M. I. Sutormina, *J. Theor. Biol.* **2008**, *252*, 247.
[57] D. V. Dibrova, M. Y. Galperin, E. V. Koonin, A. Y. Mulkidjanian, *Biochemistry* **2015**, *80*, 495.
[58] J. Foriel, P. Philippot, P. Rey, A. Somogyi, D. Banks, B. Ménez, *Earth Planet. Sci. Lett.* **2004**, *228*, 451.
[59] K. Chandru, T. Z. Jia, I. Mamajanov, N. Bapat, H. J. Cleaves, *Sci. Rep.* **2020**, *10*, 17560.
[60] A. Antunes, D. K. Ngugi, U. Stingl, *Environ. Microbiol. Rep.* **2011**, *3*, 416.
[61] T. J. McGenity, R. T. Gemmell, W. D. Grant, H. Stan-Lotter, *Environ. Microbiol.* **2000**, *2*, 243.
[62] D. Segré, B. Shenhav, R. Kafri, D. Lancet, *J. Theor. Biol.* **2001**, *213*, 481.
[63] J. M. Iglesias-Artola, B. Drobot, M. Kar, A. W. Fritsch, H. Mutschler, T. Y. Dora Tang, M. Kreysing, *Nat. Chem.* **2022**, *14*, 407.
[64] R. Yamagami, J. L. Bingaman, E. A. Frankel, P. C. Bevilacqua, *Nat. Commun.* **2018**, *9*, 2149.
[65] A. S. Petrov, J. C. Bowman, S. C. Harvey, L. D. Williams, *RNA* **2011**, *17*, 291.
[66] S. Mittal, C. Nisler, J. W. Szostak, *bioRxiv* **2023**.
[67] J. P. Chin, J. Megaw, C. L. Magill, K. Nowotarski, J. P. Williams, P. Bhaganna, M. Linton, M. F. Patterson, G. J. C. Underwood, A. Y. Mswaka, J. E. Hallsworth, *Proc. Natl. Acad. Sci. USA* **2010**, *107*, 7835.
[68] M. H. Hecht, S. P. Kounaves, R. C. Quinn, S. J. West, S. M. M. Young, D. W. Ming, D. C. Catling, B. C. Clark, W. V. Boynton, J. Hoffman, L. P. DeFlores, K. Gospodinova, J. Kapit, P. H. Smith, *Science* **2009**, *325*, 64.
[69] J. F. Mustard, S. L. Murchie, S. M. Pelkey, B. L. Ehlmann, R. E. Milliken, J. A. Grant, J. P. Bibring, F. Poulet, J. Bishop, E. N. Dobrea, L. Roach, F. Seelos, R. E. Arvidson, S. Wiseman, R. Green, C. Hash, D. Humm, E. Malaret, J. A. McGovern, K. Seelos, T. Clancy, R. Clark, D. Des Marais, N. Izenberg, A. Knudson, Y. Langevin, T. Martin, P. McGuire, R. Morris, M. Robinson, et al., *Nature* **2008**, *454*, 305.
[70] N. J. Tosca, A. H. Knoll, S. M. McLennan, *Science* **2008**, *320*, 1204.
[71] A. R. Hendrix, T. A. Hurford, L. M. Barge, M. T. Bland, J. S. Bowman, W. Brinckerhoff, B. J. Buratti, M. L. Cable, J. Castillo-Rogez, G. C. Collins, S. Diniega, C. R. German, A. G. Hayes, T. Hoehler, S. Hosseini, C. J. A. Howett, A. S. McEwen, C. D. Neish, M. Neveu, T. A. Nordheim, G. W. Patterson, D. A. Patthoff, C. Phillips, A. Rhoden, B. E. Schmidt, K. N. Singer, J. M. Soderblom, S. D. Vance, *Astrobiology* **2019**, *19*, 1.
[72] J. I. Lunine, *Acta Astronaut.* **2017**, *131*, 123.
[73] J. R. Cronin, G. W. Cooper, S. Pizzarello, *Adv. Space Res.* **1995**, *15*, 9751.
[74] S. Pizzarello, Y. Wang, G. M. Chaban, *Geochim. Cosmochim. Acta* **2010**, *74*, 6206.
[75] L. Becker, B. Popp, T. Rust, J. L. Bada, *Earth Planet. Sci. Lett.* **1999**, *167*, 71.
[76] L. M. Barge, E. Flores, J. M. Weber, A. A. Fraeman, Y. L. Yung, D. VanderVelde, E. Martinez, A. Castonguay, K. Billings, M. M. Baum, *Geochim. Cosmochim. Acta* **2022**, *336*, 469.
[77] L. M. Barge, E. Flores, D. G. VanderVelde, J. M. Weber, M. M. Baum, A. Castonguay, *J. Geophys. Res. Planets* **2020**, *125*, e2020JE006423.
[78] E. K. Leask, B. L. Ehlmann, *AGU Adv.* **2022**, *3*, e2021AV000534.
[79] J. Kimura, N. Kitadai, *Astrobiology* **2015**, *15*, 430.
[80] G. Choblet, G. Tobie, C. Sotin, M. Běhounková, O. Čadek, F. Postberg, O. Souček, *Nat. Astron.* **2017**, *1*, 841.
[81] M. Andreani, G. Montagnac, C. Fellah, J. Hao, F. Vandier, I. Daniel, C. Pisapia, J. Galipaud, M. D. Lilley, G. L. Früh Green, S. Borensztajn, B. Ménez, *Nat. Commun.* **2023**, *14*, 347.
[82] A. Zandanel, L. Truche, R. Hellmann, A. Myagkiy, G. Choblet, G. Tobie, *Icarus* **2021**, *364*, 114461.
[83] N. Khawaja, F. Postberg, J. Hillier, F. Klenner, S. Kempf, L. Nölle, R. Reviol, Z. Zou, R. Srama, *Mon. Not. R. Astron. Soc.* **2019**, *489*, 5231.
[84] W. Montgomery, E. A. Jaramillo, S. H. Royle, S. P. Kounaves, D. Shulze-Makuch, M. A. Sephton, *Astrobiology* **2019**, *19*, 711.
[85] J. M. T. Lewis, J. S. Watson, J. Najorka, D. Luong, M. A. Sephton, *Astrobiology* **2015**, *15*, 247.

